JOURNAL OF PROPULSION AND POWER
Vol. 26, No. 5, September–October 2010

Linear Stability Analysis of a Conical Liquid Sheet

Qing-fei Fu,* Li-jun Yang,† Yuan-yuan Qu,‡ and Bin Gu‡
Beijing University of Aeronautics and Astronautics, 100191 Beijing, People's Republic of China

DOI: 10.2514/1.48346

A linear instability analysis method has been used to investigate the breakup of a conical liquid sheet under the combined influence of sinuous and varicose modes of disturbances at the liquid–gas interfaces. The maximum disturbance wave growth rate of two disturbance modes has been worked out by solving the dispersion equation of a conical liquid sheet, and the corresponding angular frequencies and dominant wave numbers have been obtained. A modified model to predict the breakup length of the conical liquid sheet was adopted. Furthermore, the surface deformation curves, which can estimate how long time the breakup process will take, have been plotted by solving the surface deformation equation. For both modes, the maximum disturbances growth rate and the dominant wave number increase as the pressure drop increase, while the breakup length and breakup time decrease with the increase of the pressure drop. Although the whole conical liquid sheet presents the varicose shape when the breakup takes place, the sinuous mode dominates the breakup process. With the increase of the geometrical characteristic parameter, the breakup length and breakup time decrease. The phase angle between the two modes affects the breakup slightly. To validate the conical sheet breakup model, the experiments were performed with the injectors of different geometry characteristics parameters and a high-speed dynamic measurement system was used to grab the detailed information of the liquid sheet breakup process. Comparison with experimental results shows that the calculation results coincide with the experiments, and the present analysis provides a good starting point for predicting unstable, wave-type behavior of the conical liquid sheet.

I. Introduction

LIQUID swirl injectors are widely used in the preparation for the combustion mixtures of high-energy release devices such as rocket engines and jet engines. In a swirl injector, angular momentum is imposed on the liquid to form a swirling motion. Under the action of centrifugal force, the liquid spreads out in the form of a conical sheet as soon as it leaves the nozzle. It is well known that the disintegration of the liquid sheet is due to the growth of the unstable wave at the interface between the gas and the liquid sheet. Various forces such as aerodynamic force, inertial force, surface tension, shear force, and centrifugal force involved in the disintegration process compete to dominate the instability of the liquid sheet. If a protuberance is produced on the interface as the liquid sheet travels downstream from the nozzle owing to any disturbance, forces acting on the interfaces develop. The surface tension always tends to restore the interface back to its original equilibrium position, while the disturbance induced normal stresses, the liquid and gas generally enhance the degree of instability, i.e., increase the amplitude of the disturbance. A relative velocity between the liquid and gas promotes the growth of disturbances until the disturbance reaches the most unstable state and the liquid sheet disintegrates into fragments, which rapidly contract into unstable ligaments under the effect of surface tension. Finally, the ligaments are broken into a multitude of droplets.

There are two independent modes of unstable waves exist on the liquid–gas interface: an antisymmetric wave or the so-called sinuous mode and a symmetric wave or varicose mode. While the phase contrast of distortion on two interfaces is 180°, it is called the varicose disturbance wave (Fig. 1a). While the distortion on two liquid–gas interfaces is same-phase, it is called the sinuous disturbance wave (Fig. 1b). A previous study of the planar liquid sheets shows that the sinuous mode has a larger growth rate, and it tends to grow faster than the varicose mode, whereas, the varicose mode brings the two interfaces close together, causing the liquid sheet to breakup. This brings out the necessity of investigating the case of a conical liquid sheet to determine whether the sinuous mode or the varicose mode dominate the breakup process of a conical liquid sheet.

The breakup length is the distance between the nozzle and the place where the drop formation occurs. The breakup length is one important design parameter for combustion chamber. The matching of the breakup length of the liquid sheet and the combustion chamber length needs to be considered especially. The breakup length divided by spray velocity denotes one fraction of the combustion time delay, which can be used to predict the propellant supply system instability and the low-frequency combustion instability. Understanding the factors that influence the disintegration process will benefit not only atomizer design and improvement but also numerical simulation of spray combustion. The breakup and atomization mechanism of liquid sheet of injector has always been a fundamental study task. Although the breakup mechanism for flat liquid sheet has been understood for some time, the theory of breakup mechanism for conical sheets has yet to be developed.

Linear stability theory can evaluate the beginnings of instability of liquid sheet. It provides a good starting point for predicting unstable, wave-type behavior of the jet with disturbances. Therefore, extensive linear stability studies have been conducted in the instability of planar liquid sheets and annular sheets. In the 1970s, Lin and Kang [1] studied the atomization mechanism of a column jet in both temporal model and convective model. Crapper et al. [2] studied the linear stability of an annular liquid sheet in 1975. Shen and Li [3] applied the linear stability theory to study the breakup process of an annular viscous liquid jet exposed to both inner and outer gas streams of unequal velocities. Ibrahim [4] studied the evolution of symmetrical and anti symmetrical disturbances of a moving viscous liquid sheet in an inviscid gas medium with the spatial instability theory. Sushanta et al. [5] carried out a dual-mode linear stability analysis under the combined influence of sinuous and varicose modes of disturbance at the two liquid–gas interfaces. The effect of various parameters on the breakup characteristics of the liquid sheets had been investigated. However, they did not research on the conical liquid sheet formed by the swirl injector. Nath et al. [6] conducted a temporal stability analysis of a plane liquid sheet that is subjected to different gas velocities on both sides. Yoshinaga [7] examined the breakup and encapsulation phenomena of a gas-cored compound

Received 1 December 2009; revision received 3 March 2010; accepted for publication 6 March 2010.

*Ph.D. Candidate, School of Astronautics.
†Professor, School of Astronautics; yanglijun@buaa.edu.cn (Corresponding Author).
‡Graduate Student, School of Astronautics.

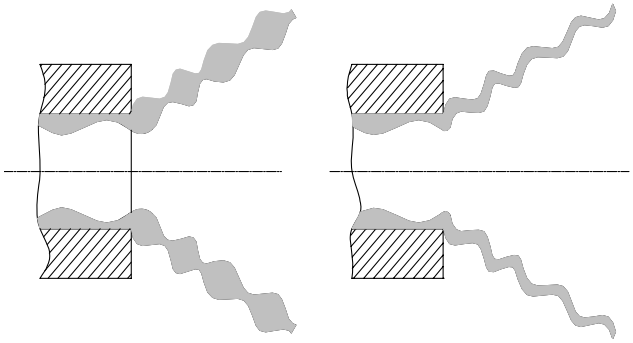

a) Varicose mode b) Sinuous mode

Fig. 1 Model of conical liquid sheet.

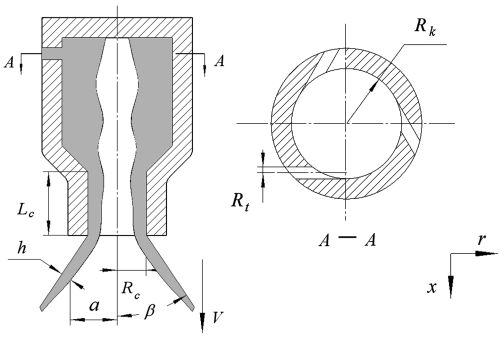

Fig. 2 Schematic of a conical liquid sheet and a swirl injector.

liquid jet, which consists of an inviscid and incompressible core gas and surrounding annular liquid.

Many efforts have also been made to study the breakup characteristics of the liquid sheet formed by the pressure-swirl injector. Liao et al. [8] developed a dispersion relation for a swirling annular liquid sheet sandwiched by swirling air streams, including the effects of viscosity. However, it is somewhat difficult to use in multidimensional models since their viscous based results required the numerical solution of a complex, nonlinear equation. Yue and Yang [9] made a linear stability analysis on the spatial instability of a conical sheet, whose method is similar to Crapper's. Mehring and Sirignano [10] analyzed the nonlinear distortion and breakup of a swirling axisymmetric thin inviscid liquid sheet in a void and at zero gravity by means of a reduced dimension approach. They found that swirl causes a reduction in breakup length and times compared with an annular sheet. Briffa and Dombrowski [11] and Dombrowski and Hooper [12] correlated the breakup length of liquid sheet on the basis of theoretical relation developed from the first order theory of Squire [13]. Inamura et al. [14] measured the sheet cone angle and breakup length of a swirl coaxial injector using photography and a contact mesh probe, and their empirical equations were deduced by modifying those of a simplex swirl injector. Kim et al. [15] studied experimentally the effect of condensation of an ambient gas on the spray characteristics and the disintegration mechanism of water sheet for the swirl spray injector.

A literature survey on the study of the conical liquid sheet breakup length is shown in Table 1. Many literatures emphasized on the effects of Weber number (ratio of the inertial and interfacial surface tension forces), Ohnesorge number (ratio of the internal viscous force to the interfacial surface tension force), and Reynolds number on the breakup characteristics of the conical liquid sheet. The types of injectors studied in these literatures can be categorized into monopropellant swirl injector and dual-propellant coaxial swirl injector. Most of the researchers measured the breakup length of the conical liquid sheet formed by different kinds of the injectors; however, they did not develop a method to predict the breakup length of the conical liquid sheet.

In this paper, to investigate the breakup characteristics of the conical liquid sheet, a linear stability model is applied to a thin liquid film generated by a swirl injector. Because the configuration of the injector has an important influence on the atomization process, the experiments were performed with different injectors to validate the conical liquid sheet breakup mode based on the linear stability analysis method.

II. Breakup Model for Conical Liquid Sheet

A. Linear Stability Analysis for Conical Liquid Sheet

For a model of a conical liquid sheet, and the derivation of dispersion relationship, refer to [2]. We consider a conical sheet with internal radius a and thickness h, as shown in Fig. 2. The initial sheet thickness at the exit of the injector is h_0, and a_0 denotes the radius of the injector spout. A constant half of the spray cone angle β along the flow direction is assumed. In the undisturbed state, the liquid in the sheet, of density ρ_l, has velocity V, and the surrounding gas, of density ρ_g, is at rest. The surface tension of liquid is σ.

Following the usual procedure, the displacement of the inner and outer surface may be taken, respectively, to be

$$\eta_1 = R\eta_{1,0}\exp[i(kx - \bar{\omega}t)] \qquad \eta_2 = R\eta_{2,0}\exp[i(kx - \bar{\omega}t)] \quad (1)$$

Where η denotes the fluctuation amplitude, subscripts 1, 2 represent the inner and outer surface of the liquid sheet, and subscript 0 means the initial state. Wave number $k = 2\pi/\lambda$, where λ is wavelength of disturbance wave, $\bar{\omega} = \bar{\omega}_r + i\bar{\omega}_i$, where real part $\bar{\omega}_r$ denotes disturbance frequency, and imaginary part $\bar{\omega}_i$ denotes the growth rate of disturbance wave. Generally it is believed that the liquid sheet will disintegrate when the disturbance wave growth rate is greatest.

The deduction of dispersion relation refers to Yue's method [9]. For incompressible irrational flow the motion is defined by the Laplace equation

$$\nabla^2\phi_i = 0 \quad (2)$$

where $i = 0$ denotes liquid film, $i = 1, 2$ correspond to the gas inside and outside of the liquid film, ϕ is the velocity potential function.

Table 1 Literature survey on study of conical liquid sheet breakup length

Number	Author	Reference	Type of injector	Geometry of injector	Ambient pressure
1	Inamura et al.	[14]	Swirl coaxial injector	Long nozzle	Without
2	Kim et al.	[15]	Pressure-swirl injector	Constant geometry	With
3	Chung et al.	[16]	Pressure-swirl injector	Geometry unknown	Without
4	Li et al.	[17]	Pressure-swirl injector	Constant geometry	Without
5	Ramamurthi et al.	[18]	Swirl injector	With a cylindrical swirler, variable geometry	With
6	Kim et al.	[19]	Liquid–liquid swirl coaxial injector	Variable geometry, with recessed length	Without
7	Ghorbanian et al.	[20]	Pressure-swirl injector	Geometry unknown	Without
8	Kim et al.	[21]	Swirl injector	Variable geometry parameter, no convergent nozzle	Without
9	Han et al.	[22]	Liquid-liquid coaxial swirl injector	With recessed length	Without
10	Hamid et al.	[23]	Swirl injector	With a cylindrical swirler, geometry unknown	Without

In the polar coordinate, the velocity potential function can be defined as follows:

$$\phi_i = RG_i(r)\exp[i(kx - \bar{\omega}t)] \quad (i = 1, 0, 2) \tag{3}$$

Substitute Eq. (3) to Eq. (2), solve it and the general solution is

$$G_i(r) = A_i I_0(kr) + B_i K_0(kr) \quad (i = 1, 0, 2) \tag{4}$$

and I_0 and K_0 are zero-order Bessel functions.

At the central axis of the air core, the radial velocity is 0 because of the symmetry. The air is at stagnation at infinite distance, so the boundary conditions are as follows for regions 1, 2:

$$v_r = \frac{\partial \phi}{\partial r} = 0, \qquad r = 0, \infty \tag{5}$$

We can get

$$B_1 = 0, \qquad A_2 = 0 \tag{6}$$

Thus, Eq. (4) changes to

$$\left.\begin{array}{l} G_1(r) = A_1 I_0(kr) \\ G_0(r) = A_0 I_0(kr) + B_0 K_0(kr) \\ G_2(r) = B_2 K_2(kr) \end{array}\right\} \tag{7}$$

On the interface of liquid and air, there is no mass transfer. The normal stress on the liquid–air interface is continuous. These boundary conditions can be expressed in mathematic representation, combining the Bernoulli equation:

$$\left.\begin{array}{c} \frac{\partial \eta_1}{\partial t} - \frac{\partial \phi_1}{\partial r} = 0 \\ \frac{\partial \eta_1}{\partial t} + V\frac{\partial \eta_1}{\partial x} - \frac{\partial \phi_0}{\partial r} = 0 \\ r = a \end{array}\right\} \tag{8a}$$

$$\left.\begin{array}{c} \frac{\partial \eta_2}{\partial t} - \frac{\partial \phi_2}{\partial r} = 0 \\ \frac{\partial \eta_2}{\partial t} + V\frac{\partial \eta_2}{\partial x} - \frac{\partial \phi_0}{\partial r} = 0 \\ r = a + h \end{array}\right\} \tag{8b}$$

$$\rho_g \frac{\partial \phi_1}{\partial t} - \rho_l\left(\frac{\partial \phi_0}{\partial t} + V\frac{\partial \phi_0}{\partial x}\right) = \sigma\left(\frac{\partial^2 \eta_1}{\partial x^2} + \frac{\eta_1}{\bar{a}^2}\right) \qquad r = a \tag{9a}$$

$$\rho_l\left(\frac{\partial \phi_0}{\partial t} + V\frac{\partial \phi_0}{\partial x}\right) - \rho_g \frac{\partial \phi_2}{\partial t} = \sigma\left(\frac{\partial^2 \eta_2}{\partial x^2} + \frac{\eta_2}{\bar{a}^2}\right) \qquad r = a + h \tag{9b}$$

where $\bar{a} = a/\cos(\beta)$.

Substitute Eqs. (1), (3), (7), and (8), eliminating A_0, A_1, B_0, B_2, $\eta_{1,0}$, and $\eta_{2,0}$, the final dispersion relation for a conical sheet can be presented as a polynomial of fourth order:

$$\begin{aligned} &\bar{\omega}^4\left[\rho_l^2(CD - EF) + \frac{\rho_l\rho_g}{k}(CN + DM) + \frac{\rho_g^2}{k^2}MN\right] \\ &- \bar{\omega}^3[4kV\rho_l^2(CD - EF) + 2V\rho_l\rho_g(CN + DM)] \\ &+ \bar{\omega}^2\left[6k^2V^2\rho_l^2(CD - EF) + kV^2\rho_l\rho_g(CN + DM)\right. \\ &\left. + \rho_l\sigma(C + D)\left[\frac{1}{\bar{a}^2} - k^2\right] + \frac{\rho_g\sigma}{k}(M + N)\left[\frac{1}{\bar{a}^2} - k^2\right]\right] \\ &- \bar{\omega}\left[4k^3V^3\rho_l^2(CD - EF) + 2kV\rho_l\sigma(C + D)\left[\frac{1}{\bar{a}^2} - k^2\right]\right] \\ &+ k^4V^4\rho_l^2(CD - EF) + k^2V^2\rho_l\sigma(C + D)\left[\frac{1}{\bar{a}^2} - k^2\right] \\ &+ \sigma^2\left[\frac{1}{\bar{a}^2} - k^2\right]^2 = 0 \end{aligned} \tag{10}$$

where

$$\begin{aligned} C &= \frac{I_0(ka)K_1[k(a + h)] + I_1[k(a + h)]K_0(ka)}{\Lambda} \\ D &= \frac{I_0[k(a + h)]K_1(ka) + I_1(ka)K_0[k(a + h)]}{\Lambda} \\ E &= \frac{1}{ka}\frac{1}{\Lambda} \\ F &= \frac{1}{k(a + h)}\frac{1}{\Lambda} \\ \Lambda &= k\{I_1[k(a + h)]K_1(ka) - I_1(ka)K_1[k(a + h)]\} \\ M &= \frac{I_0(ka)}{I_1(ka)} \\ N &= \frac{K_0[k(a + h)]}{K_1[k(a + h)]} \end{aligned}$$

The variation of the sheet thickness along the spray direction could be calculated according to mass conservation and the geometry of conical sheet. A relationship can be gotten:

$$ah = a_0h_0 \tag{11}$$

$$(a - a_0)/s = \sin(\beta) \tag{12}$$

where s denotes the length of the liquid sheet. Assume there is a relationship between s and disturbance wavelength λ in convenient, i.e., $s = C\lambda$. C is a constant relative to liquid property, injector configuration and spray pressure, and C is given by experiments [17]; h_0 is calculated with the principle of the maximum flow. The characteristic time for dimensionless is $[T] = \sqrt{\rho_l h_0^3/\sigma}$, and the characteristic length is $[L] = h_0$.

B. Breakup Length Calculation

The breakup of conical liquid sheets emerging from a swirl injector undergoes a complex, unsteady, nonlinear process, and it is an important parameter to evaluate the atomization quality. The breakup length is shorter, the primary atomization is more obscure, and the atomized liquid drop is smaller. Ligaments are assumed to form from the sheet breakup process once the unstable wave reach critical amplitude. Through solving the dispersion equation of the conical sheet, the maximum growth rate can be obtained. If the fluctuation of the liquid sheet surface has reached a value of $\eta_{\mathrm{bu}} = \eta_0 \exp(\omega_s \tau_{\mathrm{bu}})$ at breakup, a breakup time, τ_{bu}, can be evaluated:

Table 2 Configuration parameters of the model injectors

R_c/mm	R_t/mm	R_k/mm	Number of tangential channel n	$A = \frac{R_c(R_k - R_t)}{nR_t^2}$	L_c/mm
1.0	1.0	3.0	1	2	0.6
1.0	1.0	5.0	1	4	0.6

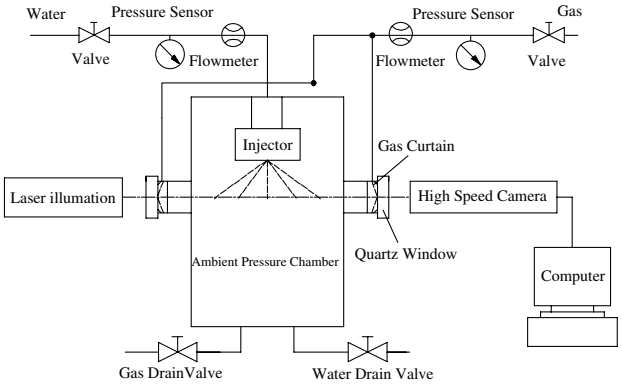

Fig. 3 Schematic diagram of the experimental system.

$$\tau_{\mathrm{bu}} = \ell_n(\eta_{\mathrm{bu}}/\eta_0)/\omega_s \tag{13}$$

where ω_s is the maximum growth rate. Thus, the sheet will break up at a length given by

$$L = V\tau_{\mathrm{bu}} = V\,\ell_n(\eta_{\mathrm{bu}}/\eta_0)/\omega_s \tag{14}$$

The quantity $\ell_n(\eta_{\mathrm{bu}}/\eta_0)$ is given the value 12 suggested by Dombrowski and Hooper [12]. However, some investigator reported that $\ell_n(\eta_{\mathrm{bu}}/\eta_0)$ is not a universal value and has to be determined experimentally in every case [15].

C. Dual-Mode Breakup Calculation

Though breakup of liquid sheet is a completely nonlinear phenomenon, a prediction of the breakup length can also be assessed by the linear analysis. On the liquid–gas interfaces, disturbances are present in the form of sinuous and varicose waves with a phase angle θ between them. Therefore, the initial condition for the surface deformation can be written as

$$\eta_j(x,0) = \eta_0[\varepsilon_1\cos(kx) + (-1)^{j+1}\varepsilon_2\cos(kx+\theta)] \tag{15}$$

where $j = 1, 2$ refers to the outside and inside interface, respectively; ε_1 and ε_2 are the weighting factors denoting a pure sinuous wave for $\varepsilon_1 = 1$ and$\varepsilon_2 = 0$, and a pure varicose wave for $\varepsilon_1 = 0$ and $\varepsilon_2 = 1$.

Then the final surface deformation equation can be expressed as follows [5]:

$$\eta_j(x,t) = \eta_0[\varepsilon_1\cosh(\bar{\omega}_{i,s}t)\cos(\bar{\omega}_{r,s}t + k_S x) + (-1)^{j+1}\varepsilon_2\cosh(\bar{\omega}_{i,v}t)\cos(\bar{\omega}_{r,v}t + k_V x + \theta)] \tag{16}$$

where $\bar{\omega}_{i,s}$ and $\bar{\omega}_{i,v}$ are the imaginary parts of ω, which represent the disturbance growth rate for the sinuous and varicose modes, respectively; $\bar{\omega}_{r,s}$ and $\bar{\omega}_{r,v}$, the real parts of ω, are the corresponding angular frequency; k_S and k_V denote the wave numbers of the sinuous and varicose modes.

III. Experimental Setup

The schematic of the experimental system is shown in Fig. 3. The experimental system is composed of simulation propellant supply system, pressure and flow measurement system, high-speed dynamic testing system. Water is used as the liquid propellants. To remove the influence of pipeline vibration, a pressurized-water supply system is adopted. High-pressure gas forces water flowing through the regulator valve to the injector. The response frequency of the pressure sensor is $0 \sim 100$ KHz, the measuring range is $0 \sim 1.5$ MPa, and the precision is 0.15%. high-speed dynamic measurement system consists of copper vapor laser light sheet illumination, Ultima-40K high-speed digital camera, control system, image analysis PC, and image analysis system. The system record and analysis the spray process at the frame rate of 4500 frames per second. This system has the temporal and dimensional statistics ability, can calculate the Sauter mean diameter, droplets size distribution and the speed of droplet. The resolution of the testing system is no less than 40 μm, with a measurement tolerance of less than 10%. The system was calibrated using standard particle board.

Injector models are made of stainless steel, whose schematic is shown in Fig. 2. Two model injectors with different geometry characteristic constants were designed. The configuration parameters are shown in Table 2. Each picture shot at the measuring point shows a projection of the measuring area, which is vertical to the axes of the injector. Figure 4 shows some continuous spray images at one measuring point shot in 5/4500 s continuously. It shows that the disturbance wave generated continuously on the surface of liquid sheet, and propagated downstream. A pressure sensor and flow meter are fixed to the pipe near the injector. When the valve of the pipe is open, the high-speed camera begins to work, saving these photographs into image analysis PC during 1 s. Experiment with different injector models under every operation condition is repeated.

IV. Results and Discussion

A. Spray Cone Angle

The spray cone angle is an important parameter in liquid rocket engine. It characterizes the spatial distribution of the liquid droplets; therefore, it has a strong influence on the combustion performance, the interaction between multi-injectors and the cooling of the injector

a)t=t_0+1/4500s **b)t= t_0+2/4500s** **c)t= t_0+3/4500s** **d)t= t_0+4/4500s** **e)t= t_0+5/4500s**

Fig. 4 Conical liquid sheet photograph shot by high-speed camera.

a) *P* =0.2 MPa **b) *P* =0.35 MPa** **c) *P* =0.5 MPa** **d) *P* =0.65 MPa** **e) *P* =0.8 MPa**

Fig. 5 Spray image of $A = 2$ injector under different pressure drop.

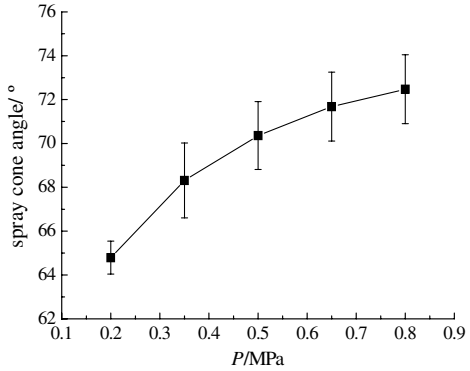

Fig. 6 Spray cone angle of $A = 2$ injector under different pressure drop.

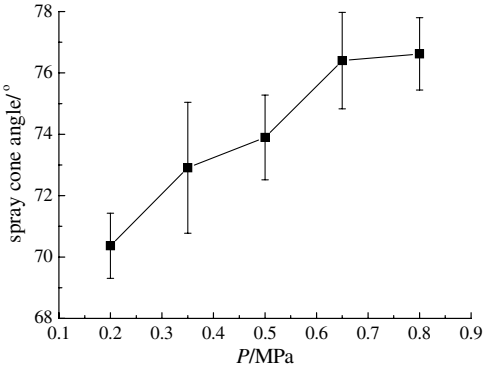

Fig. 8 Spray cone angle of $A = 4$ injector under different pressure drop.

plate in rocket engines [15]. In the present study, the spray cone angle is defined as the angle between the edges of spray cone, and the spray cone angle is measured by the postprocessing software and averaged from the shot images.

Figures 5–8 show the effects of the pressure drop and injector's geometry characteristics on the swirling liquid spray cone angle. The conical sheet in all plots seems not axisymmetric more or less. It is because that the spray is inherently a three-dimensional cone. Hence, it looks a little asymmetric in a planar picture. For the injector $A = 2$, the spray fully develops while the pressure drop exceeds 0.2 MPa. The effect of the pressure drop on spray cone angle of the injectors is shown in Figs. 6 and 8. As the pressure drop increases, the spray cone angle increases. It can also be seen from Figs. 5–8 that the spray cone angle increases as the injector's geometry characteristic parameter A increases. Because

$$A = \frac{R_{BX}R_c}{nR_T^2} = \frac{(Q/n\pi R_T^2) \times \bar{R}_{BX}}{Q/\pi R_c^2} = \frac{\text{tangential velocity} \times \text{arm coefficient}}{\text{axial velocity}} \tag{17}$$

where R_{BX} is the radius of the vortex chamber, R_C is the radius of the nozzle, R_T denotes the radius of the tangential channel, n denotes the number of the tangential and Q is the volume flow.

The liquid tangential velocity or arm of force increase as A increases, that is, the moment of momentum increase, the liquid in the swirl injector swirls more intensively. Hence, the spray cone angle increases.

Moreover, it can be seen from Fig. 5a that the spray cone contracts before the sheet breakup for the injector $A = 2$. Once the liquid sheet starts to breakup, the spray of droplets entrain ambient gas at the inner and outer surfaces of the spray. However, the inner gas volume is limited by the liquid sheet, so the pressure drop between the inner and outer gas causes the contraction of the spray. If the pressure drop becomes higher, both tangential and axial velocities increase. The contraction of the spray cone will not happen.

B. Liquid Sheet Velocity

The liquid sheet velocity V is actually the axial velocity of the liquid sheet when it emerges out of the injector. V is important because the maximum growth rate of a disturbance wave is a function

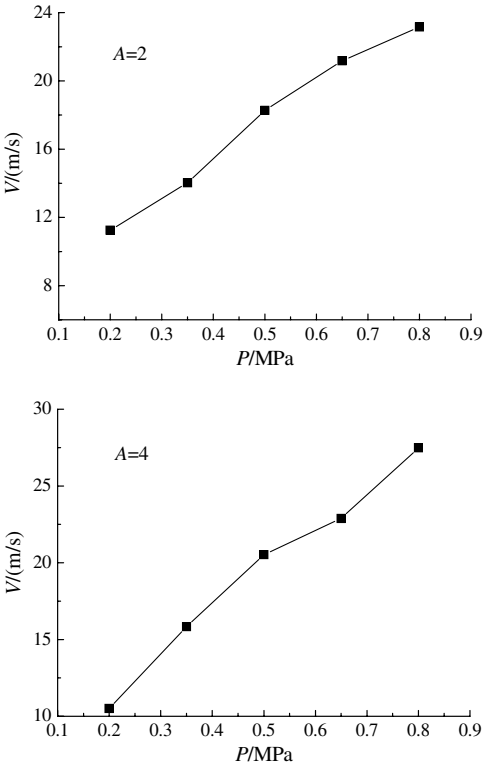

Fig. 9 Liquid sheet velocity of the model swirl injectors.

of the liquid sheet velocity, and it is required during the linear stability analysis. Actual liquid sheet velocity is different from the theoretical prediction because of the friction losses. Real liquid sheet velocity V can be obtained by dividing the axial displacement of the liquid film in two images with the time difference between the two images. The liquid sheet velocity of the two model injectors under different pressure drop are shown in Fig. 9.

It shows that the liquid sheet velocity increases slightly as the geometry characteristics parameter increase. This phenomenon can be explained by the frictional loss of the tangential velocity because

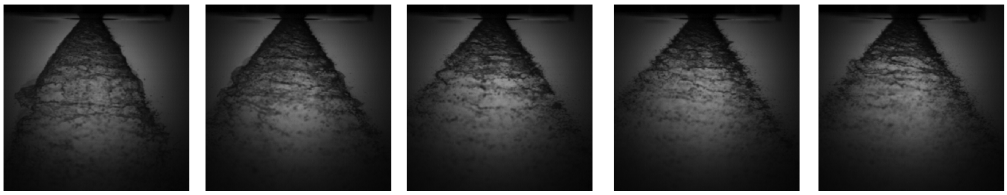

a) P =0.2 MPa **b) P =0.35 MPa** **c) P =0.5 MPa** **d) P =0.65 MPa** **e) P =0.8 MPa**

Fig. 7 Spray image of $A = 4$ injector under different pressure drop.

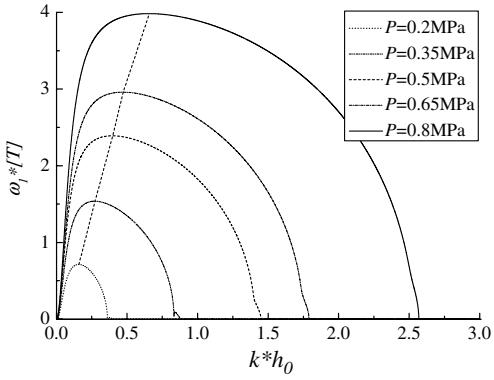

a) Sinuous model

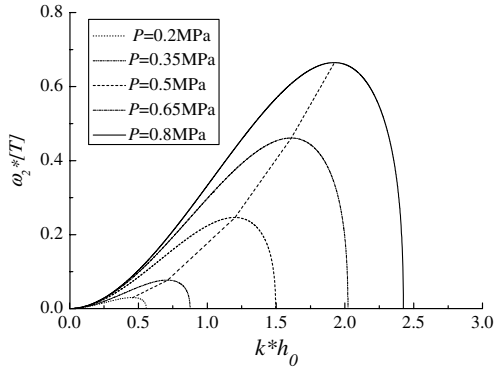

b) Varicose model

Fig. 10 Variation of growth rate with wave number ($A = 2$).

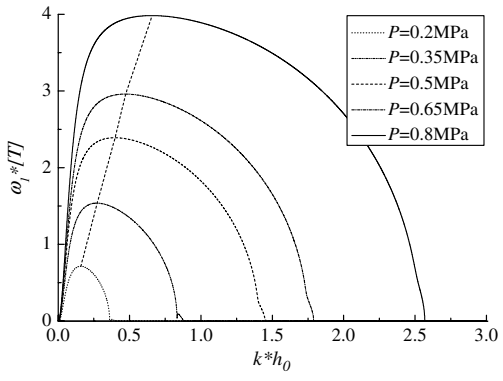

a) Sinuous model

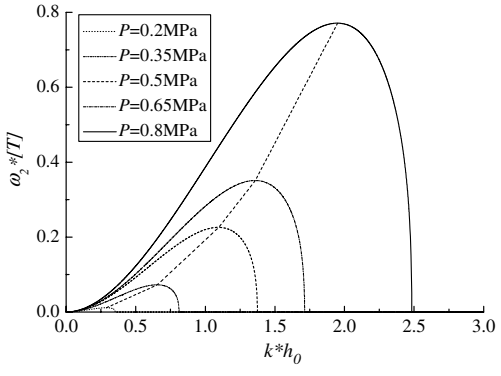

b) Varicose model

Fig. 11 Variation of growth rate with wave number ($A = 4$).

of the intensification of the swirl motion. As A increases which denotes the swirl intensity, the liquid swirl intensity increases in the vortex chamber. And this will cause the turbulence dissipation and the frictional loss increase. The effect on tangential velocity may be

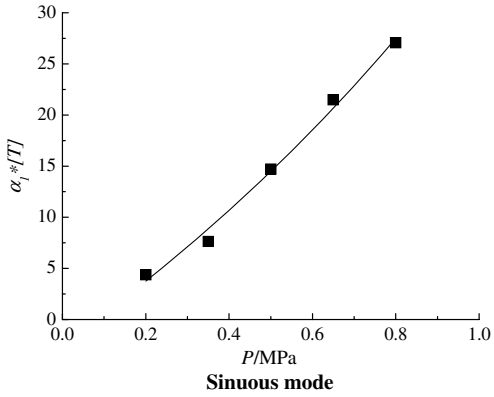

Sinuous mode

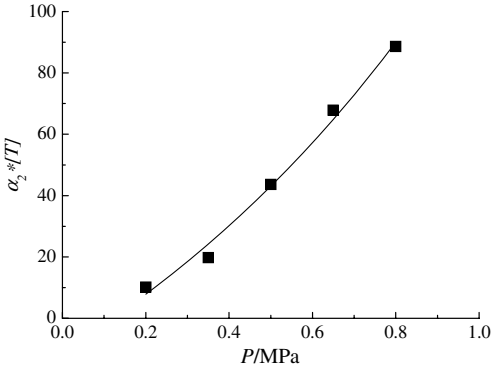

Varicose mode

A=2

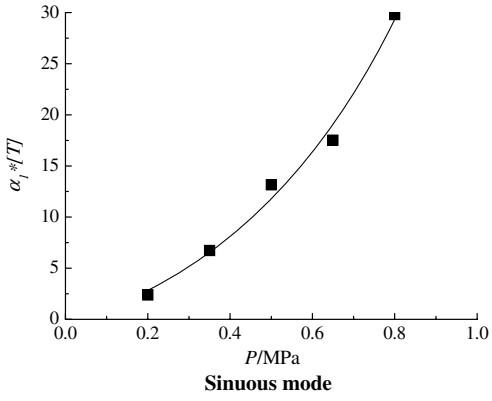

Sinuous mode

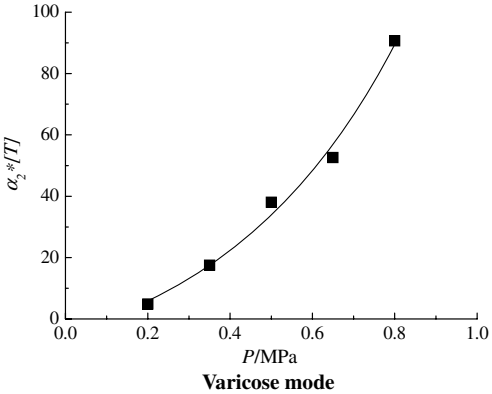

Varicose mode

A =4

Fig. 12 Variation of the angular frequency α with the pressure drop P.

greater than on the axial velocity. Hence, the liquid sheet velocities increase as A increases.

C. Linear Stability Analysis

The surface wave caused by the aerodynamic can be clearly seen on the conical liquid sheet in Figs. 5 and 7. According to the linear stability theory, the surface wave with the maximum growth rate will be the dominate wave. Figures 10 and 11 show the relation between the dimensionless wave number and dimensionless growth rate of different mode. It can be seen that the maximum growth rate and the corresponding wave number (i.e., optimum wave number) increase with the increase of pressure drop in either model. That means that the liquid sheet becomes more unstable while the pressure drop becomes higher. Consequentially, the increase of optimum wave number indicates that the wave become short wavelength mode. And this trend appears alike in different sprays of jets with different geometrical characteristic parameter. But the maximum growth rate of the surface wave is smaller for swirl injector $A = 4$ than that of the surface wave for swirl injector $A = 2$. Because the maximum disturbance wave's growth rate (imaginary part of ω) is determined, the corresponding angular frequency (real part of ω) is determined either. Figure 12 denotes the variation of the angular frequency with the pressure drop. Distinctly, the angular frequency increase with the pressure drop for both modes.

Furthermore, Figs. 10–12 show that the sinuous mode has much larger growth rate than the fundamental varicose mode. Both the sinuous and varicose modes are unstable, and they grow

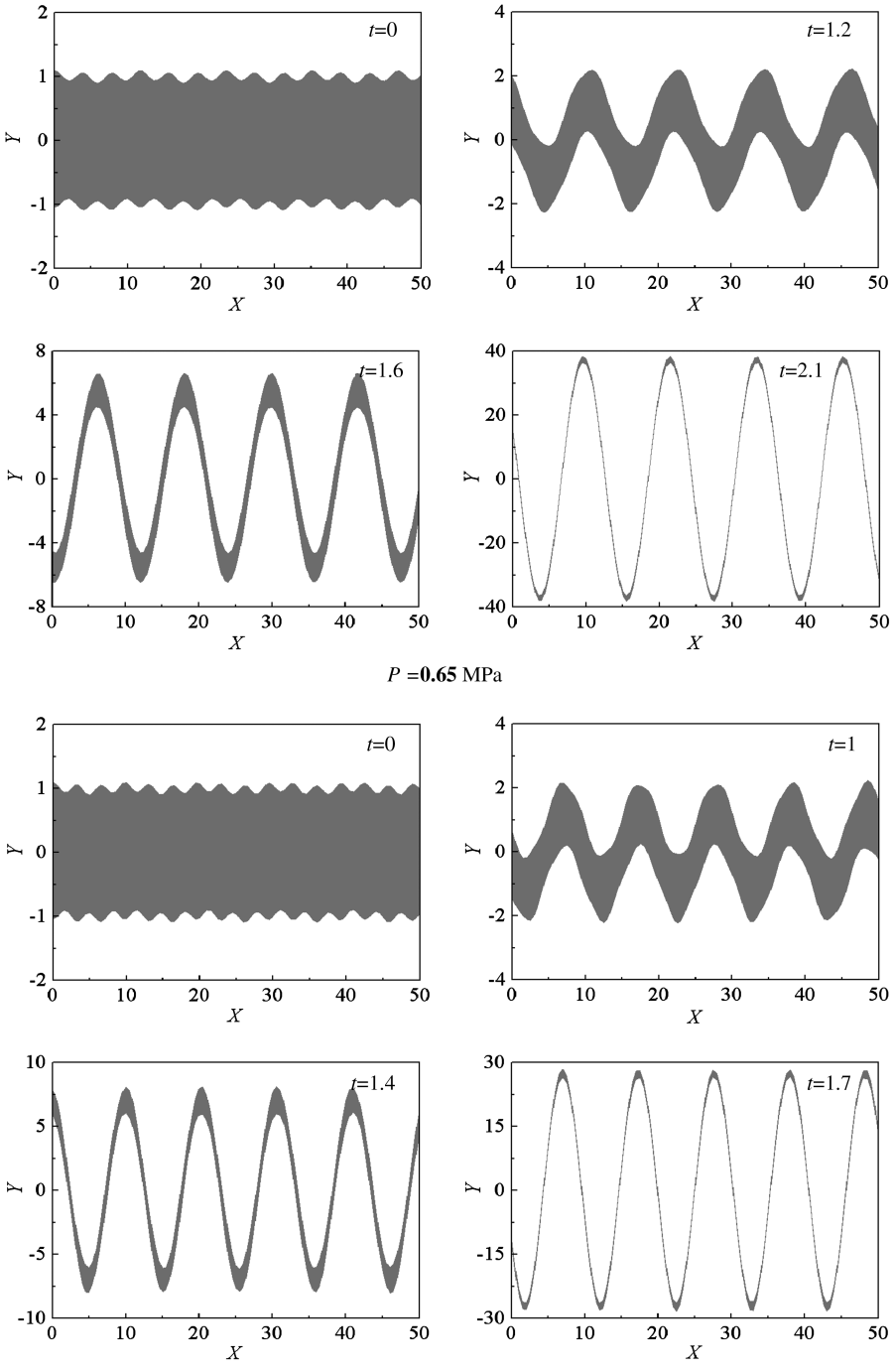

Fig. 13 The surface deformations with different pressure drops ($A = 2$, $\varepsilon_1 = 0.25$, $\varepsilon_2 = 0.75$).

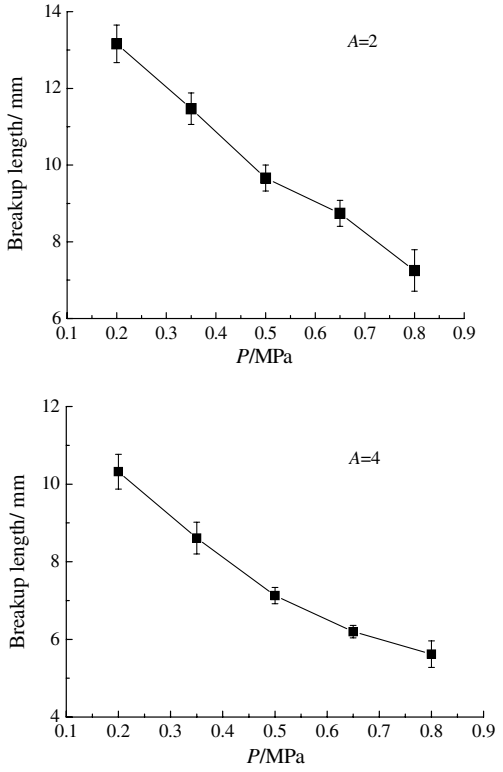

Fig. 14 Variation of breakup length with pressure drop.

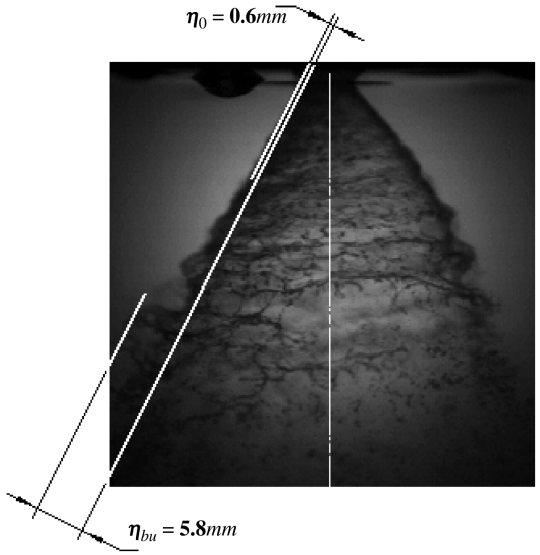

Fig. 15 Schematic of the amplitude of the disturbance on the liquid sheet.

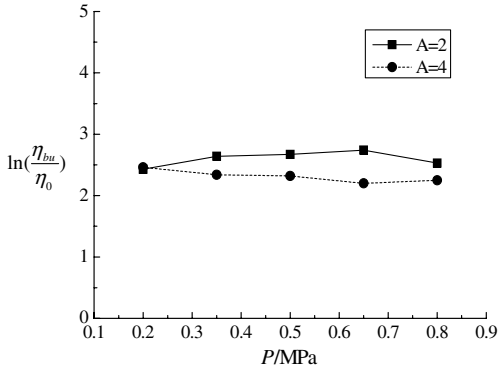

Fig. 16 Calibrated $\ell n(\eta_{bu}/\eta_0)$ according to the experiments.

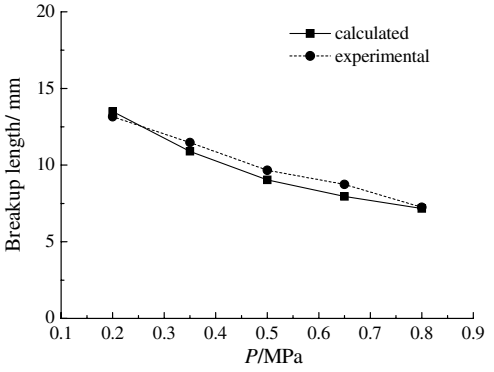

Fig. 17 Comparison of the measured breakup length and the theoretical results ($A = 2$).

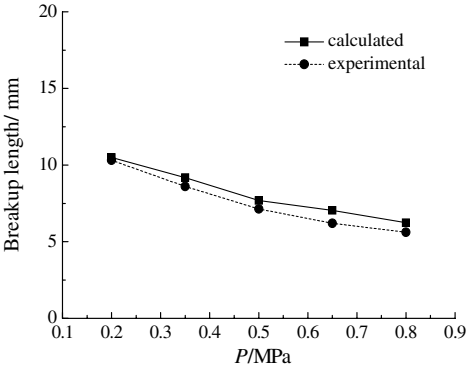

Fig. 18 Comparison of the measured breakup length and the theoretical results ($A = 4$).

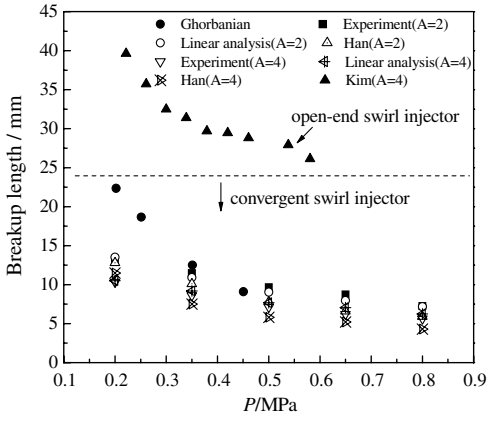

a)

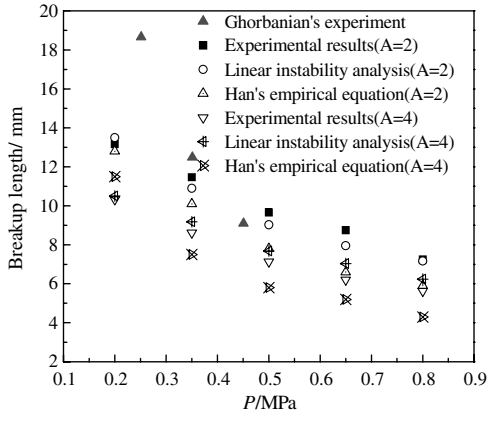

b)

Fig. 19 Breakup length with variation of injection pressure.

simultaneously in reality; but the linear stability analysis results shows that the sinuous mode is more unstable, and the surface wave tends to grow faster than the varicose mode.

D. Surface Deformation Calculation

Having gained the nondimensionalized wave numbers, disturbances growth rate, and angle frequency, the surface wave deformation at any time can be figured out based on the surface deformation equation on the liquid–gas interfaces.

Figure 13 shows the surface deformation when the geometrical characteristic parameter $A = 2$, the proportion of sinuous mode and varicose mode is 0.25 and 0.75, respectively. This series of images contains two different pressure drops: 0.65 MPa, and 0.8 MPa. For every constant pressure drop, four images at different times were listed. It can be concluded easily that the surface wave trend is to become more unstable with the time moving on, which leads to the breakup of the conical liquid sheet (in other words, the thickness of the liquid sheet almost approaches 0). Therefore, the linear instability theory can estimate the thickness of the liquid sheet and how long time the breakup process will take.

E. Breakup Length

The methods employed in the measurement of breakup length of liquid sheet from the literature may be grouped into two categories as optical method and electrical method. The optical methods can be again divided into imaging and nonimaging. The former includes flash photography and holography. The electrical methods include the method based on liquid electrical conductivity. In the photographic methods, there exists two possible ways of breakup length definition of liquid sheet for pressure-swirl nozzle in the literature. Firstly, the breakup length of the sheet has been defined as the distance from the nozzle to where the sheet is first seen to perforate. Secondly, the breakup length of the sheet can be defined as the distance from the nozzle to where the drop formation occurs. In this study, the breakup length of the liquid sheet is defined according to the second definition. The breakup length is measured from the instantaneous spray images. One hundred images are measured and averaged for one experimental case, and the deviation of data is less than 10% of their mean values. Figure 14 shows the measured liquid sheet breakup length for different injectors, and the error bar represents the standard deviation. It shows in Fig. 14 that the liquid sheet breakup length decreases with the increase of the pressure drop for both $A = 2$ and $A = 4$ injector. As the geometry characteristic A increases, the breakup length of conical liquid sheet decreases. These can be explained by two factors. Firstly, the liquid film thickness decreases with increases of injector pressure and A, and thus the liquid sheet breaks easily. Secondly, the disintegration of liquid sheet is promoted by the aerodynamic effects.

Equation (14) is used to predict the breakup length of the liquid sheet. According to Eq. (14), $L = V\,\ell_n(\eta_{bu}/\eta_0)/\omega_s$, where V can be obtained in Fig. 9, the maximum growth rate of the surface wave ω_s can be calculated according to the linear stability analysis model. Only the value of the term $\ell_n(\eta_{bu}/\eta_0)$ needs to be decided. The linear stability theory itself cannot predict critical wave amplitude for the breakup η_{bu}; hence, the term $\ell_n(\eta_{bu}/\eta_0)$ is given the value of 12 based on the work of Dombrowski and Hooper [12]. The calculation results

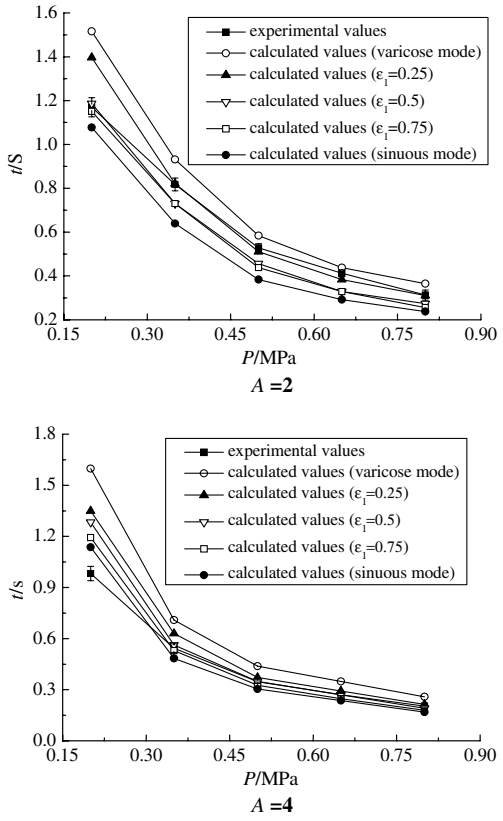

Fig. 20 The contrast between the experimental values and calculated values.

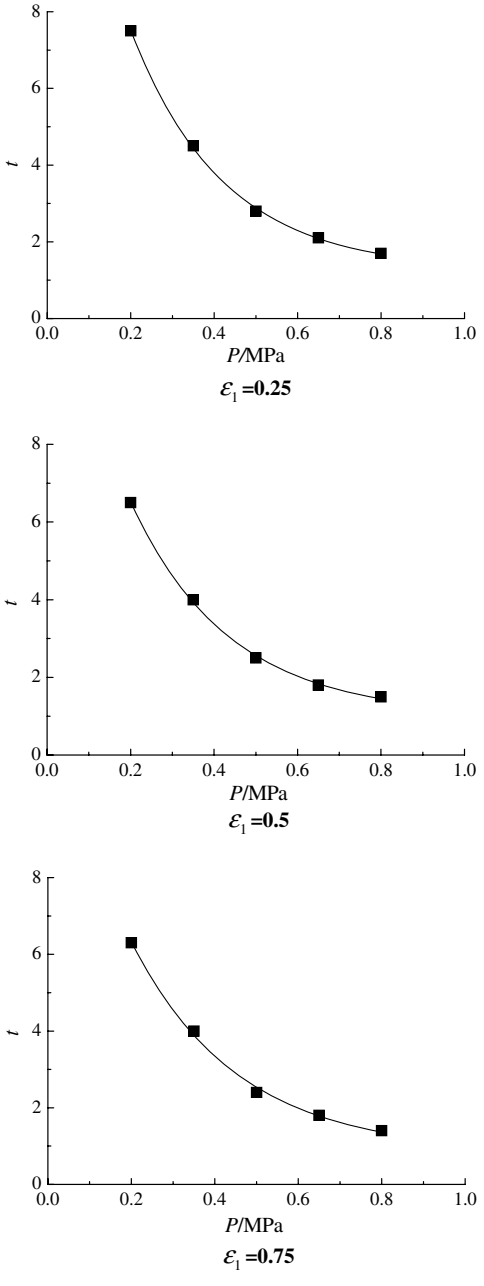

Fig. 21 Variation of the breakup time with the pressure drop ($A = 2$).

show some discrepancy of breakup length between experiments and linear stability theory. Because the critical wave amplitude for breakup is introduced from the empirical relation for the disintegration of planar liquid sheet, this value can be discrepant from the conical liquid sheet. Therefore, it is inappropriate to set the value of $\ell_n(\eta_{bu}/\eta_0)$ to be 12 in this study. It can be calibrated with the experimental data.

Figure 15 shows the measured η_{bu} and η_0 in one operating condition. In this image, the amplitude of the initial surface wave is nearly 0.6 mm, and the amplitude of the disturbance wave when the breakup take place is 5.8 mm. The term $\ell_n(\eta_{bu}/\eta_0)_{test} \approx 2.3$. Figure 16 shows the value of $\ell_n(\eta_{bu}/\eta_0)$ calculated according to the measured liquid sheet breakup length. The average value of $\ell_n(\eta_{bu}/\eta_0)$ is determined as 2.5 from the experimental data. Many studies on the breakup phenomena of liquid jet and sheet state $\ell_n(\eta_{bu}/\eta_0) = 12$ is a universal constant and can be applied to any geometrical configuration, but it seems that the term has to be determined from experiments. As a result, setting the value of $\ell_n(\eta_{bu}/\eta_0)$ to be 2.5 predicts well the breakup length of conical liquid sheet, which is shown in Figs. 17 and 18. Recent literature reported that the value of $\ell_n(\eta_{bu}/\eta_0)$ was set to be 6.9 [15] or 2 [21]. These different values of $\ell_n(\eta_{bu}/\eta_0)$ imply that $\ell_n(\eta_{bu}/\eta_0)$ should be determined according to the specified injector and working conditions. That is because η_0 changes with the geometry of the injector and the liquid flow conditions.

To establish the merit of the modified model, a comparison between our results and the known empirical equation has been done. Han et al. [24] proposed a semiempirical relation to predict the breakup length of conical liquid sheet:

$$L = C\left[\frac{\rho_L \sigma\, \ell_n(\eta_{bu}/\eta_0) h \cos\theta}{\rho_g^2 U_L^2}\right]^{0.5} \tag{18}$$

where C is an experimental constant, set to be 3 by Han. In Kim et al.'s study [21], C is modified to 0.82 based on the experimental results. They set the parameter $\ell_n(\eta_{bu}/\eta_0)$ to be 2, which is very close to our conclusion. We set the value of $\ell_n(\eta_{bu}/\eta_0)$ to be 2.5, and use Eq. (18) to validate our model and experimental results. A comparison between our linear instability analysis results and some empirical equations and experimental results in literature is

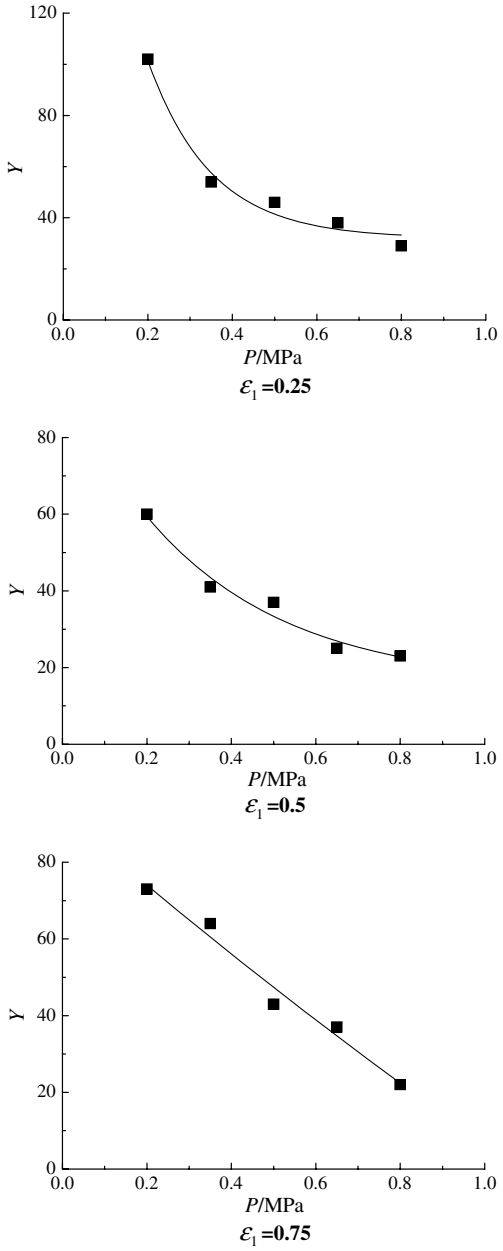

Fig. 22 Variation of the wave amplitude with the pressure drop ($A = 2$).

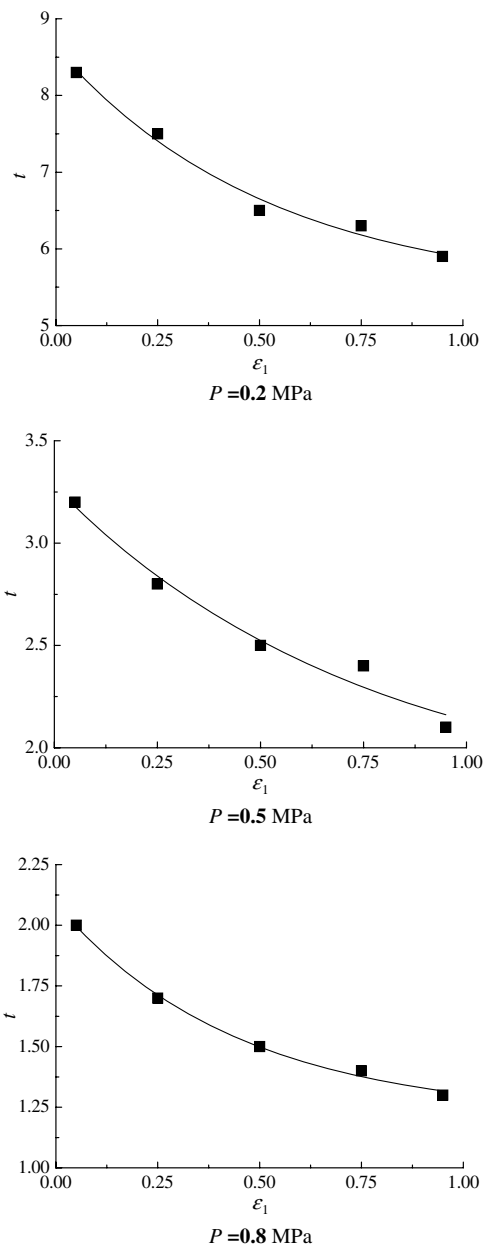

Fig. 23 Variation of the breakup time with the proportion of sinuous mode ($A = 2$).

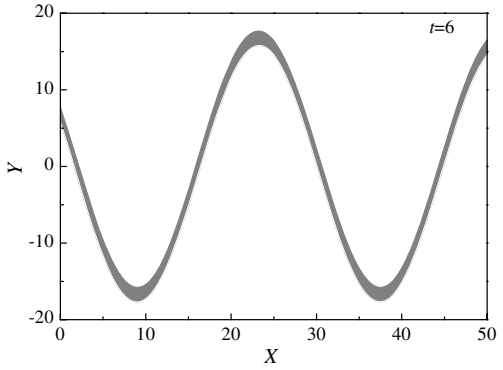

ε_1 =0.25

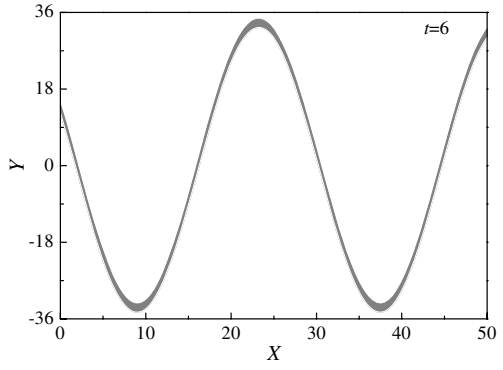

ε_1 =0.5

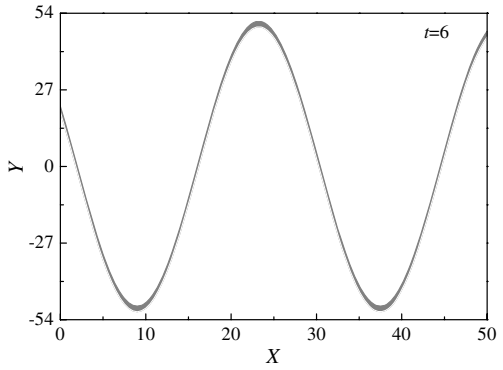

ε_1 =0.75

Fig. 24 The surface deformations when $A = 2, P = 0.2$ MPa, and ε_1 is 0.25, 0.5, 0.75 orderly.

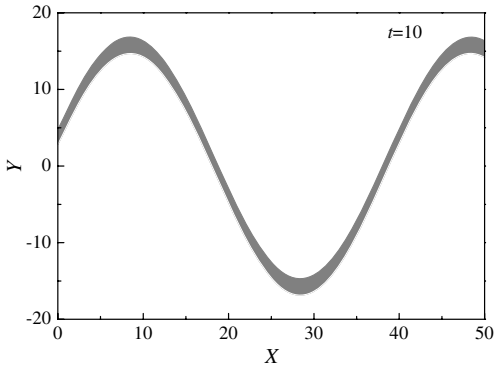

ε_1 =0.25

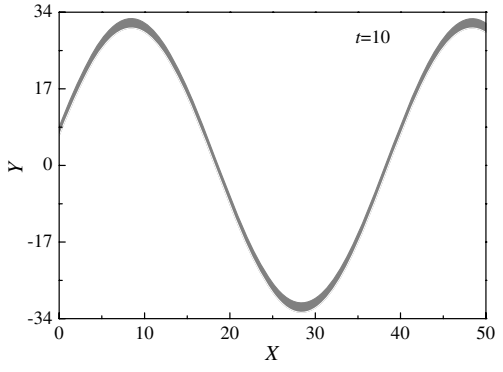

ε_1 =0.5

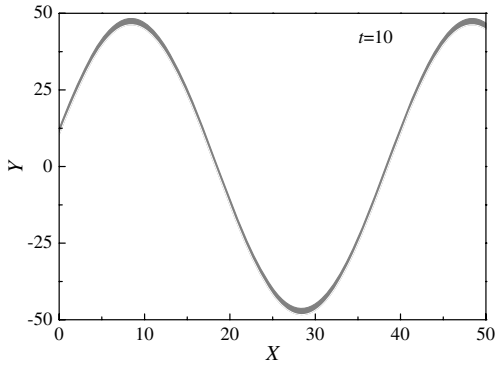

ε_1 =0.75

Fig. 25 The surface deformations when $A = 4, P = 0.2$ MPa and ε_1 is 0.25, 0.5, 0.75 orderly.

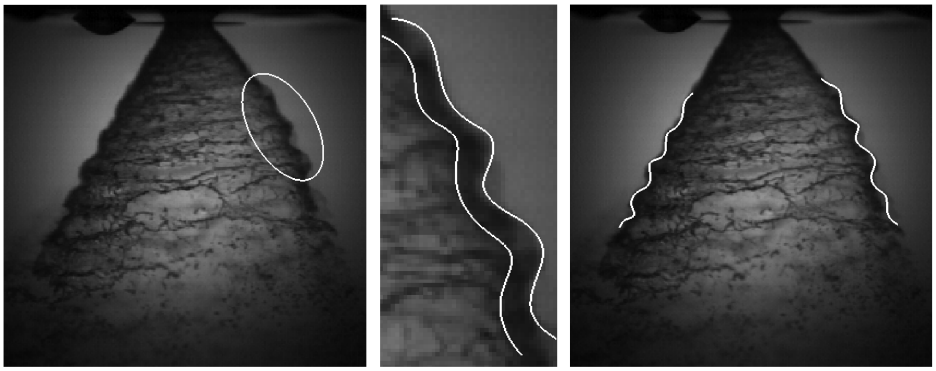

a) b) c)

Fig. 26 Photograph of the breakup of conical liquid sheet.

demonstrated in Fig. 19. Figure 19b is the magnification of the content below the dash line in Fig. 19a. Kim's experimental results deviate from other experimental results or predicted breakup length. That's because the injectors used in Kim's experiments have no convergent nozzle which are different from our injectors. The breakup length predicted with our linear analysis model agrees well with Han's empirical equations for both the $A = 2$ injector and $A = 4$ injector. Ghorbanian et al. [20] investigated the flowfield of the pressure-swirl injector for different pressure drops experimentally. The spout diameter of the injector used in Ghorbanian's experiments is the same with the swirl injector in current study, and he measured a little larger breakup length than our experimental data.

F. Breakup Time

The ratio of the measured breakup length to the measured liquid sheet velocity means the average breakup time simply. To compare the experimental breakup time and calculated values, the calculated breakup times should be multiplied by $\sqrt{\rho_l h_0^3/\sigma}$ so as to become dimensional ones. Figure 20 shows the contrast between the experimental values and the calculation values. Although it has been reported in [25] that linear instability analysis grossly underestimates the time to breakup, the images in Fig. 20 reveal that the calculated values coincide with the experiments accurately while considering the friction losses, calculative error, measurement error, and other system error, Moreover, the curves of the sinuous mode is closer to the experimental curves than that of the varicose mode, considering the conclusion of Sec. IV.C that the growth rate of the sinuous mode is much larger than that of the varicose mode, it is assumed that the sinuous mode dominates the breakup process of the conical liquid sheet.

Figures 21 and 22 show the variations of the dimensionless breakup time and dimensionless wave amplitude with the pressure drop, respectively, when the geometrical characteristic parameter $A = 2$ and ε_1 is 0.25, 0.5, 0.75. These two series of images indicate that the dimensionless breakup time and corresponding dimensionless wave amplitude decrease with the increase of the pressure drop, which means the jet pressure drop accelerates the breakup of the liquid sheet, i.e., a higher pressure drop leads to a shorter breakup time.

This trend can also be observed experimentally. According to Figs. 5 and 7, it is distinct that the breakup length decreases as the pressure drop increases. And the breakup length can denote the breakup time in a certain extent. So, it means the breakup time decreases with the increase of the pressure drop. Figure 5 also reveals that the breakup amplitude decreases as the pressure drop increases. Thus, these photos verified the former conclusion.

However, with the increase of the pressure drop, the variation curves of the breakup time trend to be smooth. In other words, the decrease of the breakup time gets smaller while the pressure drop gets higher. This means along with the increase of the pressure drop, it is more and more difficult to shorten the breakup time. Accordingly, a high pressure drop does not mean the best design. A good design should adopt the optimal pressure drop, in order to achieve the best ratio of effect to cost.

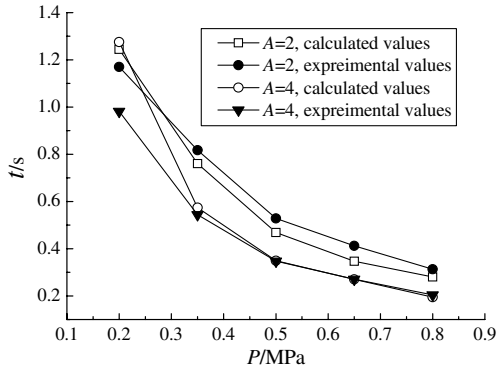

Fig. 27 Variation of the breakup time with the pressure drop.

Figure 23 describes the relationship between the dimensionless breakup time and the proportion of sinuous mode. The curves indicate a trend that when geometrical characteristic parameter is constant, the dimensionless breakup time decreases with the increase of the proportion of sinuous mode (ε_1).

Figures 24 and 25 compare the surface deformations of the sheet with different ε_1 at the same dimensionless time ($t = 6$ or 10) when other parameters are constant. Comparing these images, it is easy to get a conclusion that the wave amplitude increase with the increase of

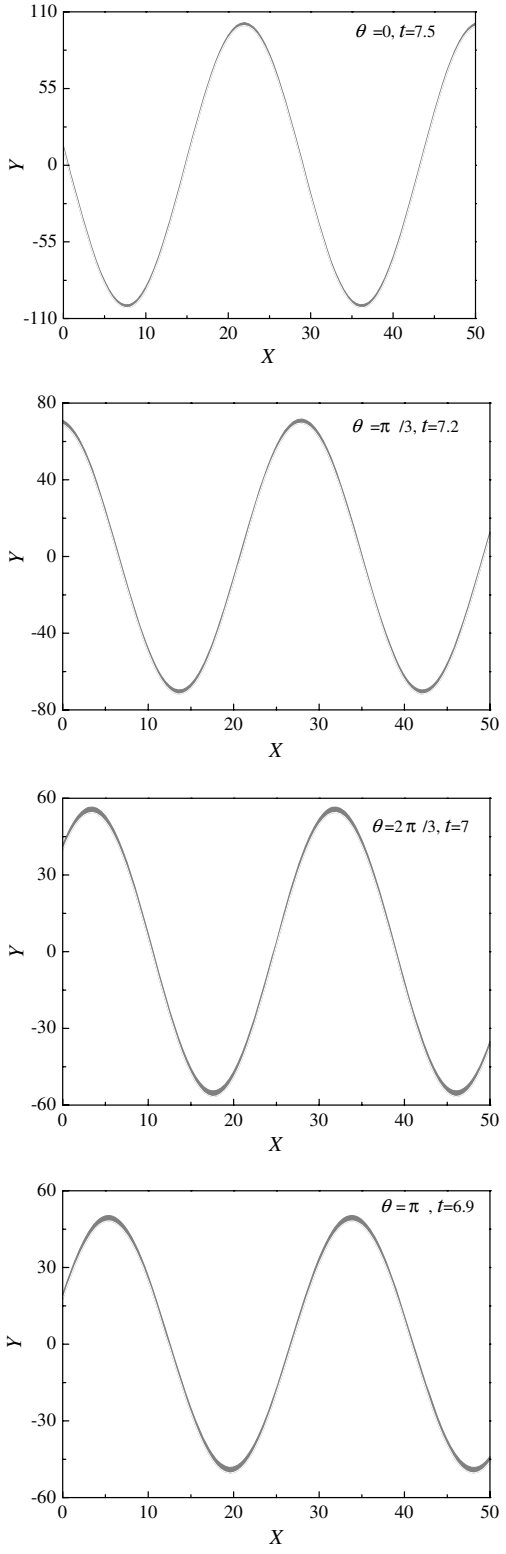

Fig. 28 The surface deformations with different phase angles between two modes.

the proportion of sinuous mode ε_1 at the uniform time. Moreover, the liquid sheet tends to become thinner, which means the breakup time tends toward shorter.

Making a comprehensive view of the foregoing information, it is evident that the sinuous mode accelerates the breakup of liquid sheet much than varicose mode. In other words, the sinuous mode dominates the breakup process of the conical liquid sheet.

This conclusion coincides with the experimental results. Figure 26 shows the photos taken in experiments. Figure 26a is the full spray photo, while Fig. 26b is the amplificatory part of the elliptical area marked on Fig. 26a. As marked by the curves in the photo, the sinuous mode wave can be distinguished from the whole spray. These photos indicate that the sinuous mode dominates the surface wave when the conical liquid sheet approaches the breakup spot nearly.

However, Sushanta et al. [5] investigated the breakup process of a plane viscous liquid sheet in a gas stream by linear stability analysis subject to the combined influence of sinuous and varicose modes, and found that the sinuous mode is responsible for the development of large amplitude deformation, whereas the varicose mode is responsible for the breakup of the liquid sheet. They also concluded that the breakup time (or length) decreases with an increase of the proportion of the varicose mode in the initial disturbance. In our study the linear stability analysis is conducted on one layer of the spray cone, and the sinuous mode dominates the breakup process. But in the whole spray cone, the varicose mode brings the two interfaces close together causing the liquid sheet to break up, i.e., considering the whole spray as a sheet, the disturbance wave presents varicose shape, which is marked in the Fig. 26c with curves.

Figure 27 shows the variation of the breakup time with the geometrical characteristic parameter. The curves of the calculated values and experimental values when $A = 2$ locate above those when $A = 4$, which means the breakup time when $A = 4$ is shorter than that when $A = 2$, i.e., the breakup time is shorter when the geometrical characteristic parameter A is larger. This trend can be observed both in the experiments and in the calculations.

Figure 28 shows the form of the liquid sheet at the time the sheet starts to breakup, while $A = 2$, $P = 0.2$ MPa, $\varepsilon_1 = 0.25$, $\varepsilon_2 = 0.75$ and the phase angle between two modes is 0, $\pi/3$, $2\pi/3$ and π orderly. These four images indicate that both breakup time and corresponding wave amplitude decrease as the phase angle between two modes increases. But the difference of the breakup time is slight, especially when the phase angle is large. This means the phase angle between two modes can accelerate the breakup of liquid sheet slightly. But this trend is difficult to observe in experiments because the phase angle cannot be controlled artificially.

V. Conclusions

A linear stability theoretical model was used to predict the breakup characteristics of a conical liquid sheet. The model considered the disturbance wave of the sinuous and varicose modes on the gas–liquid interface at the same time. Firstly, the dispersion equation of the disturbance wave was deduced and solved numerically, according to which the relation between characteristic frequency ω and wave number k was worked out. Then the maximum value of the imaginary part of ω for the two modes $\bar{\omega}_{i,s}$ and $\bar{\omega}_{i,v}$ were found out, which denoted the disturbances growth rate of the sinuous mode and the varicose mode respectively, while the maximum value of the real part $\bar{\omega}_{r,s}$ and $\bar{\omega}_{r,v}$ denoted corresponding angular frequency. The wave numbers k_S and k_V relative to $\bar{\omega}_{i,s}$ and $\bar{\omega}_{i,v}$ were the dominant wave numbers of sinuous mode and varicose mode, respectively.

The breakup length of the conical sheet was predicted with the linear stability theoretical model. At last, the surface deformation equation was solved, by which the deformation curves of the liquid sheet were plotted. To validate the sheet breakup model, two swirl injectors with various pressure drops were tested to measure their breakup lengths. Agreement between the predicted and experimental results was good for both breakup length and breakup time. All the curves were analyzed and the conclusions were obtained as follows:

1) For a conical liquid sheet, the disturbance wave growth rate of the sinuous mode is larger than that of the varicose mode. And when the proportion of the sinuous mode is larger, the breakup time is shorter, which means the sinuous mode can accelerate the breakup of the conical liquid sheet, i.e., sinuous mode dominates the breakup process of the conical liquid sheet. But for the whole spray, the spray still presents the varicose shape when the breakup takes place, because the varicose mode makes the spray cone contract and brings the two interfaces close together, causing the liquid sheet to breakup.

2) For both modes, the maximum disturbances growth rate and dominant wave number increase with the increase of the pressure drop, while the breakup length and breakup time decrease with the increase of the pressure drop. Thus, the pressure drop of jet accelerates the breakup of conical liquid sheet. However, with the increase of the pressure drop, the variation curves of the breakup time trend to be smooth.

3) While calculating the breakup length with this linear stability model, setting the value of the term $\ln(\eta_{\mathrm{bu}}/\eta_0)$ to be 12 is not appropriate; $\ln(\eta_{\mathrm{bu}}/\eta_0)$ should be approximately 2.5 in the present study.

4) Generally, the breakup length and breakup time decreases with the increase of the geometrical characteristic parameter A. The phase angle between two modes can accelerate the breakup of the liquid sheet slightly.

Acknowledgment

The financial support of China National Nature Science Funds (Support number: 50406007) and the Innovation Foundation of BUAA for Ph.D. graduates is gratefully acknowledged.

References

[1] Lin, S. P., and Kang, D. J., "Atomization of a Liquid Jet," *Physics of Fluids*, Vol. 30, No. 7, 1987, pp. 2000–2006. doi:10.1063/1.866214

[2] Crapper, G. D., Dombrowski, N., and Pyott, G. A. D., "Kelvin-Helmholtz Wave Growth on Cylindrical Sheets," *Journal of Fluid Mechanics*, Vol. 68, No. 3, 1975, pp. 497–502. doi:10.1017/S0022112075001784

[3] Shen, J., and Li, X., "Breakup of Annular Viscous Liquid Jets in Two Gas Streams," *Journal of Propulsion and Power*, Vol. 12, No. 4, 1996, pp. 752–759. doi:10.2514/3.24098

[4] Ibrahim, E. A., "Spatial Instability of a Viscous Liquid Sheet," *Journal of Propulsion and Power*, Vol. 11, No. 1, 1995, pp. 146–152. doi:10.2514/3.23852

[5] Sushanta, M. K., Li, X., Renksizbulut, M., "On the Breakup of Viscous Liquid Sheets by Dual-Mode Linear Analysis," *Journal of Propulsion and Power*, Vol. 17, No. 3, 2001, pp. 728–735. doi:10.2514/2.5802

[6] Nath, S., Mukhopadhyay, A., Sen, S., and Datta, A., "Instability Analysis of a Plane Liquid Sheet Sandwiched Between Two Gas Streams of Nonzero Unequal Velocities," AIAA Paper 2009-5157, 2009.

[7] Yoshinaga, T., "Nonlinear Instability and Encapsulation of A Compound Liquid Jet," *ILASS Americas*, Colorado, 2009.

[8] Liao, Y., Jeng, S. M., Jog, M. A., and Benjamin, M. A., "On the Mechanism of Pressure-Swirl Airblast Atomization," AIAA Paper 2001-3571, 2001.

[9] Yue, M., and Yang, M. L., "On the Spatial Instability of a Conical Sheet," *Journal of Aerospace Power*, Vol. 18, No. 6, 2003, pp. 794–798 (in Chinese).

[10] Mehring, C., and Sirignano, W. A., "Nonlinear Capillary Waves on Swirling, Axisymmetric Free Liquid Films," AIAA Paper 2000-0432, 2000.

[11] Briffa, F. E. J., and Dombrowski, N., "Entrainment of Air into a Liquid Spray," AIChE Journal, Vol. 12, No. 4, 1966, pp. 708–717.

[12] Dombrowski, N., and Hooper, P. C., "The Effect of Ambient Density on Drop Formation in Sprays," *Chemical Engineering Science*, Vol. 17, No. 4, 1962, pp. 291–305. doi:10.1016/0009-2509(62)85008-8

[13] Squire, H. B., "Investigation of the Instability of a Moving Liquid Film," *British Journal of Applied Physics*, Vol. 4, No. 6, 1953, pp. 167–169. doi:10.1088/0508-3443/4/6/302

[14] Inamura, T., Tamura, H., and Sakamoto, H., "Characteristics of Liquid Film and Spray Injected from Swirl Coaxial Injector," *Journal of*

Propulsion and Power, Vol. 19, No. 4, 2003, pp. 632–639. doi:10.2514/2.6151

[15] Kim, Dongjun., Im, Ji-Hyuk., Koh, Hyeonseok., and Yoon Youngbin., "Effect of Ambient Gas Density on Spray Characteristics of Swirling Liquid Sheets," *Journal of Propulsion and Power*, Vol. 23, No. 3, 2007, pp. 603–611. doi:10.2514/1.20161

[16] Chung, I-Ping., Presser, Cary., "Fluid Property Effects on Sheet Disintegration of a Simplex Pressure-Swirl Atomizer," *Journal of Propulsion and Power*, Vol. 17, No. 1, 2001, pp. 212–216. doi:10.2514/2.5730

[17] Li Ji-bao, Yue Ming, and Yang Mao-lin., "Experimental Research of Instability of Kelvin–Helmholtz Wave on Conical Sheets," *Journal of Aerospace Power*, Vol. 22, No. 3, 2007, pp. 337–341 (in Chinese).

[18] Ramamurthi, K., and Tharakan, T. J., "Experimental Study of Liquid Sheets Formed in Coaxial Swirl Injectors," *Journal of Propulsion and Power*, Vol. 11, No. 6, 1995, pp. 1103–1109. doi:10.2514/3.23947

[19] Kim, D., Han, P., Im, J., Yoon, Y., and Bazarov, V. G., "Effect of Recess on the Spray Characteristics of Liquid–Liquid Swirl Coaxial Injectors," *Journal of Propulsion and Power*, Vol. 23, No. 6, 2007, pp. 1194–1203. doi:10.2514/1.30450

[20] Ghorbanian, K., Ashjaee, M., Soltani, M. R., Mesbahi, M. H., and Morad, M. R., "Experimental Flow Visualization of Single Swirl Spray Pattern at Various Pressure Drops," AIAA Paper 2003-4758, 2003.

[21] Kim, D., Yoon, Y., and Han, P., "Effect of Flow Condition and Geometry on Flow Characteristics of a Swirl Injector," ILASS Americas, CA, Monterey, May 2003.

[22] Han, P. G., Seol, J., Hwang, S., and Yoon, Y., "The Spray Characteristics of Swirl Coaxial Injectors," AIAA Paper 2003-490, 2003.

[23] Hamid, A. H. A., and Atan, R., "Spray Characteristics of Jet-YSwirl Nozzles for Thrust Chamber Injector," *Aerospace Science and Technology*, Vol. 13, Nos. 4–5, 2009, pp. 192–196. doi:10.1016/j.ast.2008.10.003

[24] Han, Z., Parrish, S., Farell, P. V., and Reitz, R. D., "Modeling Atomization Processes of Pressure-Swirl Hollow-Cone Fuel Sprays," *Atomization and Sprays*, Vol. 7, No. 6, 1997, pp. 663–684.

[25] Babinsky, E., and Sojka, P. E., "Predicting Drop Size Distributions from First Principles for Non-Newtonian Fluids," *Atomization and Sprays*, Vol. 11, No. 6, 2001, pp. 597–617.

D. Talley
Editor-in-Chief